Title

Exchange bias in polycrystalline magnetite films made by ion-beam assisted deposition

Journal

Journal of Applied Physics, 116(17)

ISSN

0021-8979

Authors

Kaur, Maninder
Jiang, Weilin
Qiang, You
et al.

Publication Date

2014-11-07

DOI

10.1063/1.4900747

Peer reviewed

Exchange bias in polycrystalline magnetite films made by ion-beam assisted deposition

Maninder Kaur,[1] Weilin Jiang,[2] You Qiang,[1] Edward C. Burks,[3] Kai Liu,[3] Fereydoon Namavar,[4] and John S. McCloy[2,5]
[1]*Department of Physics, University of Idaho, Moscow, Idaho 83844, USA*
[2]*Pacific Northwest National Laboratory, Richland, Washington 99352, USA*
[3]*Department of Physics, University of California, Davis, California 95616, USA*
[4]*University of Nebraska Medical Center, Omaha, Nebraska 68198, USA*
[5]*School of Mechanical and Materials Engineering, Washington State University, Pullman, Washington 98163, USA*

(Received 15 August 2014; accepted 9 October 2014; published online 3 November 2014)

Iron oxide films were produced using ion-beam-assisted deposition, and Raman spectroscopy and x-ray diffraction indicate single-phase magnetite. However, incorporation of significant fractions of argon in the films from ion bombardment is evident from chemical analysis, and Fe/O ratios are lower than expected from pure magnetite, suggesting greater than normal disorder. Low temperature magnetometry and first-order reversal curve measurements show strong exchange bias, which likely arises from defects at grain boundaries, possibly amorphous, creating frustrated spins. Since these samples contain grains ~6 nm, a large fraction of the material consists of grain boundaries, where spins are highly disordered and reverse independently with external field. © *2014 AIP Publishing LLC*. [http://dx.doi.org/10.1063/1.4900747]

I. INTRODUCTION

Magnetite thin films with high degree of crystallinity and quantifiable nanograin size-dependent optical, magnetic, and semiconducting properties have been intensively studied. Magnetite has the inverse cubic spinel structure, where the superexchange interaction between Fe^{3+} and Fe^{2+} ions in the A and B sites make this material a promising candidate for application in semiconductor spintronics. Also, this material can operate efficiently at room temperature due to its high Curie temperature ($T_C \sim 860$ K), and relatively high electronic conductivity.[1]

Different fabrication techniques have been used to produce thin films of magnetite, such as sputtering,[2] molecular beam epitaxy,[3] electron beam evaporation,[4] and pulsed laser deposition on various substrates (MgO, $MgAl_2O_4$, $SrTiO_3$, and sapphire).[5] Ion beam assisted deposition (IBAD) is employed here, where thin films are produced by simultaneous combination of a physical vapor deposition (PVD) method and an independent ion beam bombardment.[6] This method is typically used to independently control the film composition and adhesion between the substrate and coating film.

Some unusual characteristics have been reported in single phase magnetite thin films. Antiferromagnetic coupling between the adjacent magnetite grains has been observed in magnetite thin film synthesized by ion beam assisted sputtering.[7] Some iron oxide thin films prepared by radio frequency magnetron sputtering show more than one phase, the details of which are controlled by the bias voltage.[1] In other systems, oxygen ion implantation in single phase ferromagnetic thin films[8,9] and oxidation of grain boundaries can lead to unexpected exchange bias.[10] Here, we report an unusual exchange bias effect in magnetite thin films on silicon substrates which nominally show absence of a second crystalline phase.

II. EXPERIMENTAL PROCEDURE

Magnetite thin films were grown on a silicon substrate using an IBAD[11] system (Mill Lane Engineering, Lowell, MA) at the Nanotechnology Laboratory in the University of Nebraska Medical Center.[12] Ion enhanced processes employ energetic ion bombardment to "stitch" films to the substrate during deposition, resulting in more adherent coatings than those produced without ion bombardment.

Nanocrystalline films of iron oxide were prepared by electron beam evaporating 99.98% pure iron target (Alfa Aesar) at a rate of 1.1 Å/s onto a silicon substrate. The ion beam consisted of oxygen and argon species at a constant current density of 100 μA/cm^2, energy of 500 eV, and the total operating pressure in the chamber was $\sim 4 \times 10^{-4}$ Torr including partial pressure of argon, oxygen, and vaporized atoms, in this case vapor iron. The substrate temperature reached ~110 °C due to ion beam heating during deposition.

Film physical properties were thoroughly characterized by various techniques. A Philips X'pert Multi-Purpose Diffractometer with Cu K_α radiation at 5° incident angle was used for performing glancing incidence X-ray diffraction (XRD). Rutherford backscattering spectroscopy (RBS) was performed with 2.0 MeV He^+ ions at 150° using the 3.0 MV tandem accelerator [NEC 9SDH-2 pelletron at Pacific Northwest National Laboratory (PNNL)]. Samples were prepared for transmission electron microscopy (TEM) by focused ion beam (FIB) extraction of cross-sections, and energy dispersive spectroscopy (EDS) was performed on the samples for elemental mapping. Raman spectroscopy was conducted using a Horiba HR800 high-resolution confocal

Raman microscope, with 532 nm HeNe laser for excitation, delivering approximately 20 mW power to the sample. Magnetic force microscopy (MFM) was performed using multimode atomic force microscopy (AFM, Veeco Digital Instruments, Nanoscope IIIA), a cobalt-coated probe tip (MESP, 70 kHz), and a lift height of ~20 nm.

Low temperature magnetic properties of the samples were obtained with a vibrating sample magnetometer (VSM, Quantum Design Physical Property Measurement System). Magnetization versus field (hysteresis loop to ±30 kOe) was collected at 10 K and 77 K after various cooling fields (H_{FC}) (0, 0.1, 1, 10, and 30 kOe), and loop iterations (4 cycles). First-order reversal curves (FORC)[13–16] to ±15 kOe were measured using a MicroMag 3900 VSM (Princeton Measurements Corp.) at 300 K and at 77 K with zero-field cooling (ZFC) and field cooling (FC) under 1 kOe or 10 kOe (i.e., $H_{FC} = 0$, 1 kOe, 10 kOe). The measurement starts from positive saturation and involves measuring a series of partial hysteresis curves at progressively more negative reversal field H_R under increasing applied field H back to positive saturation. A FORC distribution is then extracted from the magnetization M(H, H_R) according to[17]

$$\rho(H, H_R) = -\frac{1}{2}\frac{\partial^2 M(H, H_R)}{\partial H \partial H_R}. \quad (1)$$

The FORC distribution may also be presented in coordinates of local coercivity $H_C = (H\text{-}H_R)/2$ and bias/interaction field $H_B = (H + H_R)/2$.

III. RESULTS AND DISCUSSION

RBS determined that the Fe_3O_4 film was ~300 nm thick based on the assumed density of 5.197 g/cm^3. XRD determined the films to be polycrystalline magnetite (Fig. 1) with an average crystallite size of ~6 nm. Two important observations were made from the XRD pattern: (1) there appeared to be lattice expansion of the Fe_3O_4 and (2) all Fe_3O_4 peaks were shifted towards lower angles. The higher angle peaks shifted more compared to lower angles. The calculated lattice constant of IBAD Fe_3O_4 sample is 8.45 Å which was considerably higher than typical reported Fe_3O_4 nanoparticles with lattice constants 8.322 – 8.398 Å.[18,19] Assuming a nominal Fe_3O_4 lattice parameter of 8.398 Å, the lattice expansion of the IBAD Fe_3O_4 was calculated as ~ 0.6%. No other phases were immediately evident, but since the average crystallite size is small, causing broad diffraction peaks, minor phases with overlapping peaks (such as γ-Fe_2O_3) cannot be definitively excluded. An important possibility that may account for the range of lattice constants obtained by different researchers was the presence of oxygen in excess of the stoichiometric formula requirements.[18]

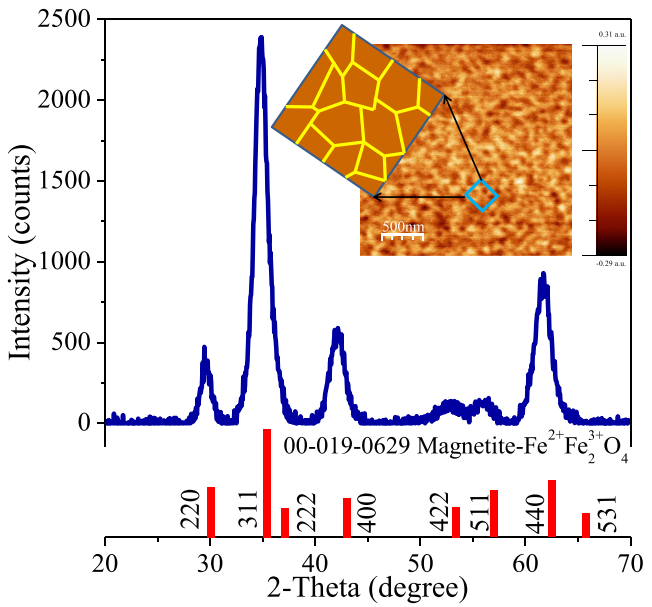

FIG. 1. XRD of IBAD film showing the broad peaks of magnetite phase. The inset figure is the corresponding MFM image representing the polygrain behavior of thin film. The zoomed-in view is a schematic of the MFM.

Raman spectra suggested that the film was heterogeneous, with areas of diffuse deposition and other areas with localized large accumulations. Spectra from areas of diffuse deposition show a broad (~75 cm^{-1}) peak at 669 cm^{-1}, with two weaker but equally broad peaks at 535 and 308 cm^{-1}. Spectra from the localized accumulations were very weak and dominated by strong scattering which increased with increasing wave number; however, peaks can be assigned to magnetite (668 cm^{-1} A_{1g}, 541 cm^{-1} T_{2g}, 311 cm^{-1} T_{2g})[20] with no other phases evident. MFM conducted at room temperature on the sample in a remnant state after saturation showed no evidence of second phase at grain boundaries within the resolution of the instrument, but does suggest that the polycrystalline films have single-domain grains (Fig. 1, inset).

TEM chemical analysis by EDS of cross-sections showed high concentrations of Ar (~4.8 at. %) in a 3–5 nm thick region at the Si/film interface. The bulk film, which consisted of columnar grains oriented perpendicular to the substrate, also had significant Ar content (~2 at%). Since samples have such small grains, a large fraction of the sample consists of grain boundaries. Along grain boundaries, there is a misalignment of the atomic structure. This misalignment may induce strains, or simply increase disorder. Typically, spins near grain boundaries are highly disordered,[21] and the presence of this additional Ar could potentially introduce more disorder. Additionally, atomic ratios measured by EDS in the bulk film away from the interface showed Fe/O of ~0.44 as compared to 0.72 for a magnetite sample prepared by a gas aggregation technique.[19] This comparison showed that the IBAD Fe_3O_4 film is significantly oxygen-rich compared to the ideal stoichiometry of ~0.75 in magnetite. There was no contribution from the Si substrate in the form of SiO_2 as the substrate was cleaned by an *in-situ* argon ion beam before deposition. It is likely that the ion beam used for synthesis of the magnetite film contributed a significant part of oxygen in the film in excess of stoichiometric magnetite.

The room temperature hysteresis loop showed no appreciable exchange bias and a coercive field H_{cf} of ~300 Oe, as shown in Fig. 2(d). The FORC distribution is shown in Fig. 2(a). The prominent FORC feature was centered at local

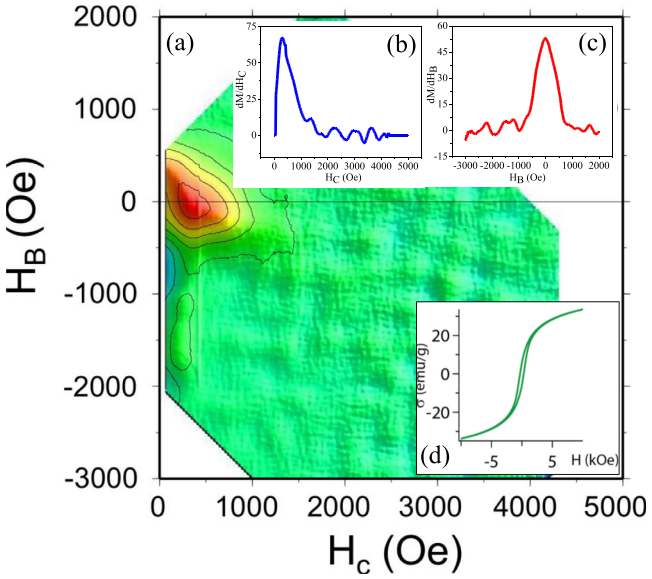

FIG. 2. (a) The room temperature FORC distribution, and its projection onto the (b) local coercivity and (c) bias field axis. (d) Hysteresis loop at 300 K.

coercivity $H_C = 400$ Oe [Fig. 2(b)] and bias field $H_B = 0$ [Fig. 2(c)], confirming the absence of exchange bias.

Interestingly, for the measurements where the sample was cooled to 77 K (both ZFC and FC), the FORC distributions all exhibited a clear shift to $H_B < 0$, as shown in Figs. 3(a)–3(d), indicating the establishment of exchange bias.[2,22] The local coercivity H_C increased substantially from the room temperature value [Fig. 3(e)]. The FORC distribution also evolved into an asymmetric "boomerang" shape and became negatively biased, similar to patterns seen in systems exhibiting strong exchange interactions.[13] In certain systems such as discrete or isolated nanomagnets,[23,24] dipolar interactions may also influence the FORC distribution. However, the dipolar field is usually modest and insensitive to temperature variations. In the present case, the magnetite films are continuous and we expect the exchange interaction to play a dominant role. Furthermore, the shift of the FORC distribution along the H_B axis is substantial, in agreement with the exchange bias determined conventionally from the major hysteresis loop, and sensitively depends on the temperature. These results conclusively demonstrate that the shift in the FORC distribution is due to the exchange bias, not dipolar interaction.

Additionally, there was minimal difference in shape of the bias (H_B, y-axis) and local-coercivity (H_C, x-axis) components of the FORC distribution with different cooling fields at 77 K (below the Verwey transition in magnetite), as observed in previous studies.[19,25] Hysteresis loops at 77 K taken independently of FORC measurements [Fig. 3(f)] showed symmetric loops and very little difference with field cooling, other than possibly the first loop iteration.

Hysteresis loops were also measured at 10 K (see Figs. 4 and 5). The first loops traced at 77 K [Fig. 3(f)] were more symmetrical in shape with weaker exchange bias fields (H_{ex}) compared to the first loops at 10 K for the same cooling field (e.g., see Fig. 5). This suggested that symmetrical behavior comes from the free rotation of grain boundary spins due to thermal effects along the direction of applied field, while the asymmetrical shape of curve was due to reversal magnetization mechanisms of frozen interfacial spins. Disordered grain boundary spins responded to external field and temperature, and reversed independently from each other.[26] As the spins were canted in this region, alignment was achieved only under strong external fields.

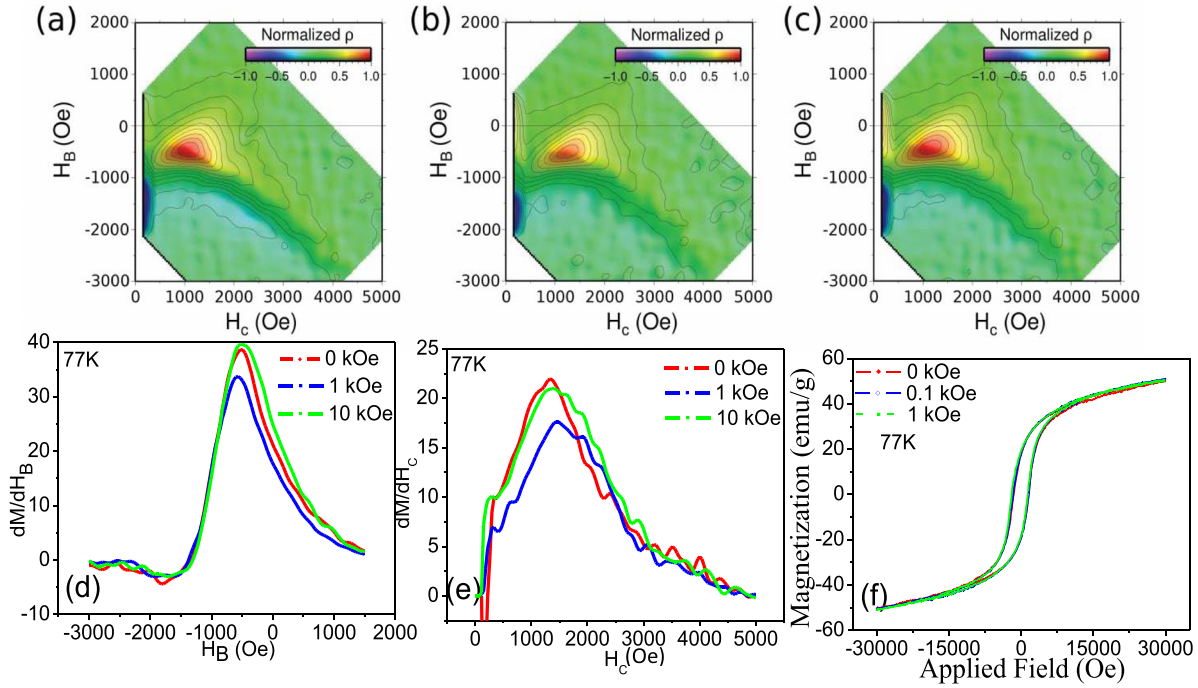

FIG. 3. FORC distributions at 77 K after cooling in (a) $H_{FC} = 0$ kOe (zero field cool), (b) $H_{FC} = 1$ kOe, and (c) $H_{FC} = 10$ kOe. Projections of the three FORC distributions onto the (d) bias field and (e) local coercivity field axis are shown for comparison. (f) First iteration hysteresis loops at 77 K.

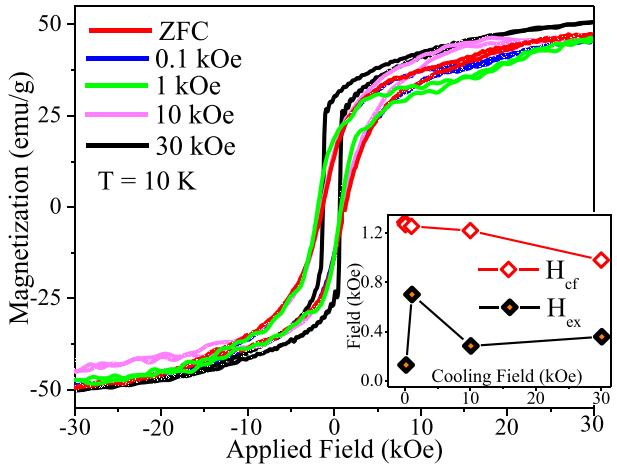

FIG. 4. Fourth iteration hysteresis loops at 10 K. Inset figure represents corresponding coercive field and exchange bias field (in kOe) with respect to different cooling fields.

The saturation magnetization increased with larger cooling fields as shown in Fig. 4, indicating that in the highly polycrystalline film, each grain contributed a different magnitude of anisotropy depending on the direction of its orientation. Hence, the net anisotropy was the sum of all the grains that were randomly aligned. Samples appeared to be unsaturated even at 30 kOe, likely due the ferrimagnetic nature of Fe_3O_4.[27] The estimated saturation magnetization is low compared to theoretical magnetite, however, probably a result of the low Fe/O ratio in the film.

In order to display exchange bias, a system must contain at least two exchange-coupled phases: one magnetically soft phase plus one magnetically hard phase that cannot be reversed in the field range of measurements. In this Fe_3O_4 film, presence of strong H_{ex} (~1500 Oe) at 10 K indicated that some other phase must be involved. We postulate that the secondary phase was present at grain boundaries in the form of amorphous or weakly crystalline γ-Fe_2O_3, due to its similar peaks in the XRD spectrum and lower than expected values for Fe/O compared to magnetite. The amount of this phase was below the detection limit of currently considered structural and imaging characterization instruments and is possibly non-crystalline.

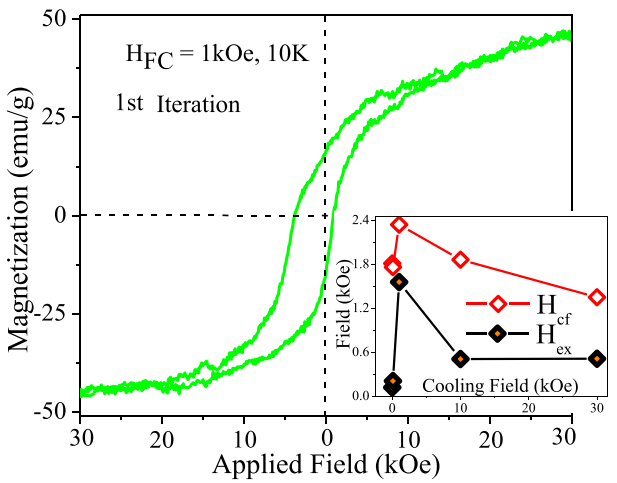

FIG. 5. First iteration hysteresis loops at 10 K for field cooling in 1kOe. Inset figure represents coercive field and exchange bias field (in kOe) with respect to different cooling fields.

Under ZFC (from demagnetized state), the spins were frozen in random directions, and respond to increasing measurement field. The exchange anisotropy was averaged out due to random orientation of spins, and hence, in the ZFC loop at 10 K, no loop shift was observed. Following the field-cooling process, the spins started freezing along the direction of field and were pinned at the grain boundaries. Due to the enhancement in the alignment degree of the Fe_3O_4 moments, the different contributions to the exchange anisotropy summed together and a net exchange bias was observed. Therefore, the hysteresis curve obtained at different cooling fields showed behavior depending on the number of frozen pinned spins. When the applied field reversed, the frozen grain boundary spins resisted rotating along the applied field. Here, the Zeeman energy became less than the magnetocrystalline anisotropy energy. The cooling field of 1 kOe caused greater anomaly in hysteresis as it demonstrated strong bias effect compared to other cooling fields (Fig. 5). Very similar results were observed in a granular system of core-shell Fe/Fe-oxide nanoclusters.[28]

A strong influence of the cooling field on the exchange bias effect was observed in the case of polycrystalline magnetite thin film. The inset of Figure 5 illustrates the dependence of H_{ex} and H_{cf} on H_{FC}. Both H_{ex} and H_{cf} of magnetite thin film were observed to increase first and then decrease with increasing H_{FC}. At low cooling field, the Zeeman energy is weak, the cooling field itself is not sufficient to reverse the spins with a random distribution of easy axis. The increase in H_{cf} with H_{FC} up to 1 kOe (Fig. 5, inset) was consistent with the increase in H_{ex}; the field cooling induced a preferential direction along which the spins tend to freeze at 10 K, and thus the effect of averaging of the anisotropy, due to randomness, was reduced. The maximum of $H_{ex} = 1.56$ kOe is achieved for the cooling field $H_{FC} = 1$ kOe. With further increase of H_{FC}, the Zeeman coupling between the field and the grain boundary spins increased as well, hence the frozen grain boundary spins gradually follow the motion of the grain spins and orient along the field direction. It causes a decrease of H_{ex}.

At 10 K, for high enough fields, such coupling competed with the mix of magnetic interactions within the system, overcoming the exchange coupling at the interface between Fe_3O_4 grain and grain boundary. The field $H_{FC} = 1$ kOe can be considered an effective depinning threshold field, above which magnetic interactions were overcome by the Zeeman coupling. Above this field, due to Zeeman coupling, the grain boundary and the grain were less strongly exchange coupled, and thus, the grain boundary exerted a weaker pinning on the grain spins, resulting in a decrease of H_{ex} and H_{cf}. If H_{FC} is strong enough, the exchange coupling can be destroyed entirely and frozen boundary spins will be rotated coherently with the grain spins, and consequently, hysteresis loop becomes symmetrical.

The film is trained by increasing the number of loop cycles while measuring the exchange bias and coercivity at 77 K and 10 K. The variation of these quantities as a function

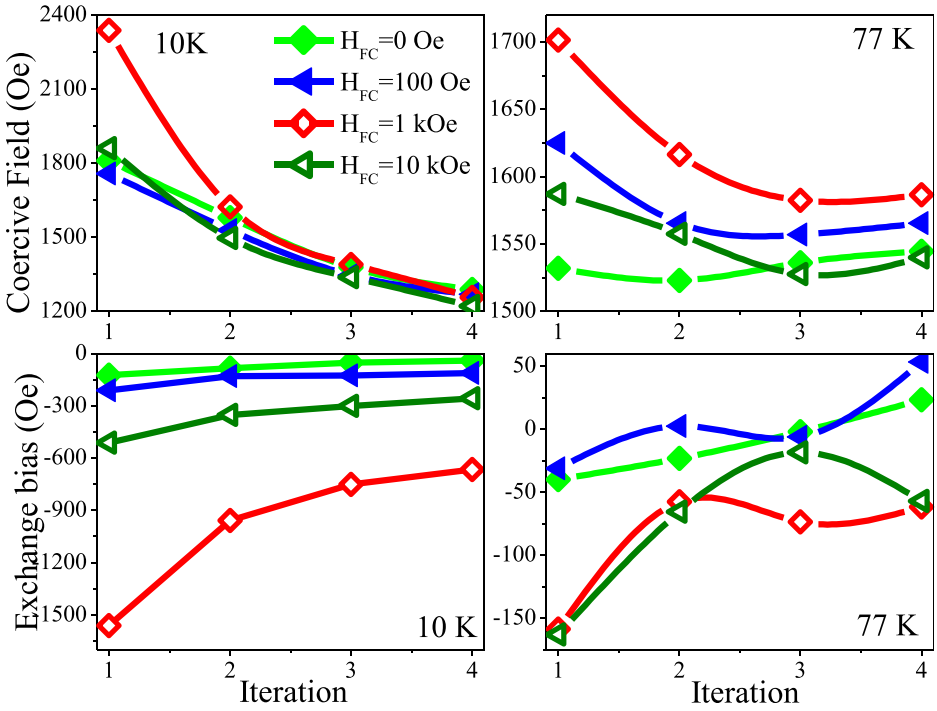

FIG. 6. Training effect shown for hysteresis loops at 10 K and 77 K, taken after FORC measurements. Note that absolute values of H_{ex} as well as differences in loop-to-loop are much smaller for 77 K than for 10 K.

of loop cycles was a direct macroscopic fingerprint of configurational rearrangements of the spin structure towards equilibrium. A clear training effect was seen in the variation of H_{ex} and H_{cf} (Fig. 6), where both parameters decreased with increasing loop cycles. Some of the frozen spins which were aligned in the cooling field direction changed their directions and fell into other metastable configurations during field cycling, resulting in a decrease of H_{ex} during field cycling. A fraction of frozen spins that are depinned from their initial alignment and canted in off-axis directions with each magnetic field cycle can be observed by comparing 1st and 4th iteration curves (Figs. 4 and Fig. 5). The anomaly in the 1st iteration curve disappeared during subsequent cycles.

IV. CONCLUSION

These films produced by IBAD were shown by TEM-EDS to be significantly oxygen-rich, though no other phase is apparent in XRD or Raman spectroscopy. It is highly probable that the grain boundaries of this material contain oxygen-rich non-crystalline iron oxides (e.g., Fe_2O_3) that give rise to the strong exchange bias effect observed at 10 K. Additionally, it was seen that the film itself, and particularly the interface to the substrate, was highly enriched in Ar due to the ion bombardment inherent in IBAD. The presence of this Ar in the film may influence the grain boundary structure and lead to increased potential for exchange bias due to other iron oxide stoichiometries.

ACKNOWLEDGMENTS

This work was supported in part by Laboratory Directed Research & Development and in part by NSF (DMR-1008791). The Pacific Northwest National Laboratory (PNNL) is operated for the U.S. Department of Energy (DOE) by Battelle under Contract DE-AC05-76RL01830. Some of the research was performed using the Environmental Molecular Sciences Laboratory (EMSL), sponsored by the DOE's Office of Biological and Environmental Research and located at PNNL. The authors thank the following for assistance with characterization and helpful discussions: Alicia Certain and Matt Olszta for FIB/TEM, A. Scott Lea for MFM, Paul Gassman for Raman, Tim Droubay for magnetometry, and Tamas Varga for XRD data analysis.

[1]B. Mauvernay, L. Presmanes, C. Bonningue, and P. Tailhades, J. Magn. Magn. Mater. **320**, 58 (2008).
[2]M. Kaur, J. S. McCloy, W. Jiang, Q. Yao, and Y. Qiang, J. Phys. Chem. C **116**, 12875 (2012).
[3]F. C. Voogt, T. T. M. Palstra, L. Niesen, O. C. Rogojanu, M. A. James, and T. Hibma, Phys. Rev. B **57**, R8107 (1998).
[4]S. Jain, A. O. Adeyeye, and D. Y. Dai, J. Appl. Phys. **95**, 7237 (2004).
[5]S. B. Ogale, K. Ghosh, R. P. Sharma, R. L. Greene, R. Ramesh, and T. Venkatesan, Phys. Rev. B **57**, 7823 (1998).
[6]J. K. Hirvonen, in *Mater. Process. Surf. Interface Eng.* (Springer, 1995), pp. 307–346.
[7]A. Kumar, D. K. Pandya, and S. Chaudhary, J. Appl. Phys. **111**, 073901 (2012).
[8]J. Demeter, E. Menéndez, A. Schrauwen, A. Teichert, R. Steitz, S. Vandezande, A. R. Wildes, W. Vandervorst, K. Temst, and A. Vantomme, J. Phys. D: Appl. Phys. **45**, 405004 (2012).
[9]J. Demeter, E. Menéndez, K. Temst, and A. Vantomme, J. Appl. Phys. **110**, 123902 (2011).
[10]K. D. Sung, Y. A. Park, M. S. Seo, Y. Jo, N. Hur, and J. H. Jung, J. Appl. Phys. **112**, 033915 (2012).
[11]J. K. Hirvonen, in *Mater. Process. Surf. Interface Eng.*, edited by Y. Pauleau (Springer, Netherlands, 1995), pp. 307–346.
[12]F. Namavar, C. L. Cheung, R. F. Sabirianov, W.-N. Mei, X. C. Zeng, G. Wang, H. Haider, and K. L. Garvin, Nano Lett. **8**, 988 (2008).
[13]J. E. Davies, J. Wu, C. Leighton, and K. Liu, Phys. Rev. B **72**, 134419 (2005).
[14]J. E. Davies, O. Hellwig, E. E. Fullerton, G. Denbeaux, J. B. Kortright, and K. Liu, Phys. Rev. B **70**, 224434 (2004).
[15]R. K. Dumas, K. Liu, C.-P. Li, I. V. Roshchin, and I. K. Schuller, Appl. Phys. Lett. **91**, 202501 (2007).
[16]X. Kou, X. Fan, R. K. Dumas, Q. Lu, Y. Zhang, H. Zhu, X. Zhang, K. Liu, and J. Q. Xiao, Adv. Mater. **23**, 1393 (2011).

[17]I. D. Mayergoyz, *Mathematical Models of Hysteresis* (Springer-Verlag, New York, 1991).
[18]E. Z. Basta, Mineral. Mag. **31**, 431 (1957).
[19]W. Jiang, J. S. McCloy, A. S. Lea, J. A. Sundararajan, Q. Yao, and Y. Qiang, Phys. Rev. B **83**, 134435 (2011).
[20]S. Tiwari, D. M. Phase, and R. J. Choudhary, Appl. Phys. Lett. **93**, 234108 (2008).
[21]A. Gupta, G. Q. Gong, G. Xiao, P. R. Duncombe, P. Lecoeur, P. Trouilloud, Y. Y. Wang, V. P. Dravid, and J. Z. Sun, Phys. Rev. B **54**, R15629 (1996).
[22]J. Olamit, K. Liu, Z.-P. Li, and I. K. Schuller, Appl. Phys. Lett. **90**, 032510 (2007).
[23]D. A. Gilbert, G. T. Zimanyi, R. K. Dumas, M. Winklhofer, A. Gomez, N. Eibagi, J. L. Vicent, and K. Liu, Sci. Rep. **4**, 4204 (2014).
[24]J.-W. Liao, R. K. Dumas, H.-C. Hou, Y.-C. Huang, W.-C. Tsai, L.-W. Wang, D.-S. Wang, M.-S. Lin, Y.-C. Wu, R.-Z. Chen, C.-H. Chiu, J. W. Lau, K. Liu, and C.-H. Lai, Phys. Rev. B **82**, 014423 (2010).
[25]C. Carvallo and A. Muxworthy, Geochem. Geophys. Geosyst. **7**, Q09003 (2006).
[26]P. Lecoeur, P. L. Trouilloud, G. Xiao, A. Gupta, G. Q. Gong, and X. W. Li, J. Appl. Phys. **82**, 3934 (1997).
[27]K. Liu, L. Zhao, P. Klavins, F. E. Osterloh, and H. Hiramatsu, J. Appl. Phys. **93**, 7951 (2003).
[28]M. Kaur, J. S. McCloy, and Y. Qiang, J. Appl. Phys. **113**, 17D715 (2013).